ATLAS PUB Note
ATL-PHYS-PUB-2025-017
30th March 2025

ATLAS projected sensitivities for the cross-section measurement and new physics searches in four-top-quark production at the HL-LHC

The ATLAS Collaboration

This note presents projections for four-top-quark ($t\bar{t}t\bar{t}$) production physics results at the High-Luminosity LHC (HL-LHC) using a dataset of up to 3 ab^{-1}, collected by the ATLAS experiment. When combining ATLAS and CMS datasets, the total integrated luminosity could reach 6 ab^{-1}. The study extrapolates theoretical and experimental systematic uncertainties from Run 2 ATLAS analyses, which were conducted using 140 fb^{-1} of data, and evaluates them under two different scenarios. Sensitivity to the standard model cross-section is evaluated, along with constraints on the top-quark Yukawa coupling and limits on Wilson coefficients in the Effective Field Theory framework. In addition, the search sensitivities to various heavy-resonance particles mediating $t\bar{t}t\bar{t}$ production are estimated. In the most optimistic scenario, the expected uncertainty in the four-top-quark production cross-section is projected to be 6%, while the 95% confidence level upper limits on production cross-sections reach below 1 fb for heavy resonances with masses around or above 1 TeV.

1 Introduction

The production of four top quarks ($t\bar{t}t\bar{t}$) is a rare process in the Standard Model (SM) of particle physics. The predicted cross-section is approximately 13 fb in proton–proton (pp) collisions with a centre-of-mass energy of $\sqrt{s}$ = 13 TeV at the Large Hadron Collider (LHC) [1]. This process was recently observed for the first time by both the ATLAS [2] and the CMS [3] experiments using data from LHC Run 2. The large centre-of-mass energy required to produce $t\bar{t}t\bar{t}$ events makes them naturally sensitive to new physics effects, especially those at high energy scales. These new physics effects can be formulated either in an effective field theory (EFT) framework, such as SMEFT [4], or with dedicated beyond-the-SM (BSM) theories that predict additional heavy resonances that mediate $pp \to t\bar{t}t\bar{t}$ production. A group of these models are constructed by extending the SM Higgs sector, such as two-Higgs-doublets models (2HDM) [5], which predict additional heavy scalar (H) and pseudo-scalar (A) particles. Other top-philic resonances mediating $pp \to t\bar{t}t\bar{t}$ production are postulated, including colour-singlet vector or colour-singlet/octet scalar bosons [6–10]. These heavy new resonances are motivated by composite Higgs models [11–16], models based on minimal flavour violation [17, 18], and extended supersymmetry models [19–34].

This note presents the prospects for measuring the SM $t\bar{t}t\bar{t}$ production cross-section and searching for new physics using $t\bar{t}t\bar{t}$ events at the High-Luminosity LHC (HL-LHC) in pp collisions with $\sqrt{s}$=14 TeV. The projections are based on an integrated luminosity of 3 ab^{-1} of pp collision data, corresponding to the amount of data expected to be recorded and usable for physics analyses by ATLAS over the full HL-LHC operation period. The combined ATLAS and CMS datasets are expected to reach a total of 6 ab^{-1}[35]. The projections are based on the results obtained using the full Run 2 pp collision data with $\sqrt{s}$=13 TeV collected by the ATLAS experiment, corresponding to an integrated luminosity of 140 fb^{-1} or 139 fb^{-1}, depending on the luminosity calibration available at the time of the analyses. The projection of the SM $t\bar{t}t\bar{t}$ cross-section measurement is based on the analysis using events with two same-sign leptons[1] and more than two leptons (2LSS/ML) [2]. Various BSM interpretations in the context of the top-Higgs Yukawa coupling and the EFT are also included. Searches for heavy resonances in $t\bar{t}t\bar{t}$ events are extrapolated using the search for $pp \to t\bar{t}H/A \to t\bar{t}t\bar{t}$ production [36], where the heavy H/A bosons are predicted in the 2HDM. The search uses events with one lepton or two opposite-sign leptons (1L/2LOS), and is combined with the previous search using 2LSS/ML events [37].

2 Summary of the analyses using ATLAS Run 2 data

The SM $t\bar{t}t\bar{t}$ measurement [2] is performed with events with high multiplicities of light-flavour jets, and heavy-flavour (b-tagged) jets, as well as a large overall event activity. The event activity is probed by the scalar sum of the transverse momentum of the isolated leptons and jets, denoted by H_T. At least one of the leptons is required to have a transverse momentum above 28 GeV. A signal region is defined by selecting events with at least six jets with transverse momentum above 20 GeV, among which at least two are b-tagged jets; H_T is above 500 GeV. In this signal region, SM $t\bar{t}t\bar{t}$ events are separated from the background events using a multivariate discriminant by combining several input observables into a Graph Neural Network (GNN). Several SM processes produce events with topologies similar to $t\bar{t}t\bar{t}$ production. The dominant background arises from the production of $t\bar{t}$ accompanied by additional particles such as jets or bosons, including $t\bar{t}H$+jets, $t\bar{t}Z$+jets, and $t\bar{t}W$+jets. Theoretical modeling of the $t\bar{t}W$+jets background at high jet multiplicities suffers from significant uncertainties. To address this, a data-driven approach determines the

[1] 'Lepton' in this note refers exclusively to electron or muon.

normalisation in jet bins, while event characteristics are modelled using simulation. Additional sources of background include events with misidentified leptons or incorrect charge assignments, as well as those involving non-prompt leptons originating from heavy-flavour decays, photon conversions, or misidentified jets. Heavy-flavour decays are the primary source of non-prompt muons, while photon conversions and jet misidentification predominantly affect electrons. Background events with charge-misidentified, fake and non-prompt leptons mainly originate from $t\bar{t}$ events. The dominant systematic uncertainties in this measurement stem from the $t\bar{t}t\bar{t}$ signal modeling, with the choice of the Monte Carlo (MC) generator being the largest, followed by the effects of the parton shower and hadronisation. The uncertainties in the data-driven background estimate of $t\bar{t}W$+jets also contribute significantly. Among the experimental uncertainties, the largest arise from b-jet tagging and the jet energy scale.

The heavy resonance search in the 1L and 2LOS channel [36] is performed in events with at least seven and five jets, respectively, and with at least two b-tagged jets. The events are then categorised into orthogonal regions with exclusively seven (five) to nine (seven) jets or inclusively $\geq$ 10 ($\geq$ 8) jets, and various b-tagging requirements up to $\geq$ 5 ($\geq$ 4) b-tagged jets in the 1L (2LOS) channel. The main background after the selection is $t\bar{t}$+jets production. Data-driven corrections are applied to the simulated $t\bar{t}$+jets events. These include corrections to the kinematic properties and the normalisation of $t\bar{t}$ production in association with jets originating from b- and c-quarks. A multivariate (MVA) discriminant based on GNN [38] is used to enhance the separation of the signal from the background events. The search in the 2LSS/ML channels [37] uses a similar strategy as the measurement of the SM $t\bar{t}t\bar{t}$ production [2] with a few exceptions. The prediction of the main background from $t\bar{t}W$+jets is based on MC simulation. The normalisation of $t\bar{t}W$+jets is treated as a free parameter and determined in the profile likelihood fit for the signal extraction. An uncertainty of 133% (208%) is assigned to $t\bar{t}W$+jets events with seven (eight or more) jets, derived based on the discrepancy between data and simulation observed in a $t\bar{t}W$+jets validation region. For signal-background discrimination, boosted decision trees (BDT) are used. Two separate BDTs are trained, the first to discriminate SM $t\bar{t}t\bar{t}$ events to all other background. This BDT is used to select from the signal region a more $t\bar{t}t\bar{t}$-enriched region, within which a second BDT is used to separate $t\bar{t}H/A \rightarrow t\bar{t}t\bar{t}$ events from the SM $t\bar{t}t\bar{t}$ events. All channels are combined in a simultaneous profile likelihood fit. The dominant systematic uncertainties come from the modelling of $t\bar{t}$+jets and $t\bar{t}W$+jets backgrounds in the 1L/2LOS and 2LSS/ML channels, respectively, as well as the modelling of the SM $t\bar{t}t\bar{t}$ background.

3 Extrapolation to HL-LHC conditions

The extrapolation to HL-LHC conditions involves scaling the expected cross-sections from 13 TeV to 14 TeV for all processes. It is performed under two scenarios that reflect different assumptions about the evolution of systematic uncertainties and detector performance, with statistical uncertainties scaled according to luminosity. The first scenario, referred to as "Scenario 1" (S1), closely mirrors the 140 fb^{-1} analysis [2]. In this scenario, all systematic uncertainties are maintained at their Run 2 levels. Several free parameters are measured in the profile likelihood fit to the data when extracting the signals in the Run 2 analyses in the 2LSS/ML channel. These include parameters related to the modelling of $t\bar{t}W$+jets production and the normalisation of fake / non-prompt backgrounds. These parameters are set to their post-fit values from the corresponding Run 2 analyses to more accurately reflect the expected background contribution. The uncertainties in these parameters depend on the available data, i.e., they are scaled according to the integrated luminosity. In the second scenario, referred to as "Scenario 2" (S2), the treatment of systematic uncertainties incorporates various improvements over the 140 fb^{-1} analysis. The uncertainty arising from the choice of $t\bar{t}t\bar{t}$ generator is removed given its large overlap with other modelling uncertainties. The

other modelling systematic uncertainties are assumed to be halved compared to their Run 2 values, and instrumental uncertainties are assumed to scale with luminosity. Uncertainties in data-driven background estimates arising from the limited amount of data are scaled according the integrated luminosity. Several data-driven uncertainties are based on the discrepancies between data and predictions. These uncertainties are kept the same as the 140 fb^{-1} analysis. The only exception is the uncertainty in $t\bar{t}W$+jets events with seven or more jets in the resonance search within the 2LSS/ML channel. These uncertainties are assumed to be half of the values used in the Run 2 analysis, reflecting the expected improvements in the modelling of $t\bar{t}W$+jets production.

Table 1 and 2 list the detailed assumptions on the systematic uncertainty assumptions in S2 for the analyses used in the projection. Table 1 contains information for both the SM $t\bar{t}t\bar{t}$ measurement and the resonance search in the 2LSS/ML channel. Table 2 summarises the same information for the resonance search in the 1L/2LOS channel.

3.1 Extrapolation of the Standard Model cross-section measurement

The expected uncertainty on the $t\bar{t}t\bar{t}$ cross-section as a function of the integrated luminosity per experiment is shown in Figure 1, comparing two scenarios of systematic uncertainty treatment. The projection indicates that the uncertainty will become significantly lower than the current theoretical SM cross-section [39] after around 1 ab^{-1} per experiment in S2. For luminosities above 250 fb^{-1} per experiment, systematic uncertainties dominate. With 3 ab^{-1}, the expected systematic uncertainties in the $t\bar{t}t\bar{t}$ cross-section is 17%, which could be reduced to 7% with improved systematics. Combining ATLAS and CMS datasets could further lower it to 6%.

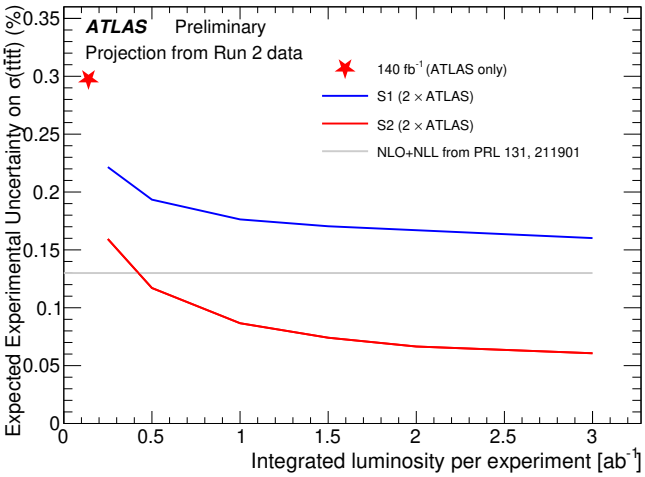

Figure 1: Expected uncertainty on the $t\bar{t}t\bar{t}$ cross-section as a function of the integrated luminosity per experiment. The blue and red curves correspond to two different scenarios of systematic uncertainty treatment (S1 and S2). The red star represents the ATLAS-only result using 140 fb^{-1} [2] from Run 2. The precision of the combined ATLAS and CMS result is approximated by doubling the integrated luminosity of a single experiment. The gray line indicates the theory uncertainty (NLO+NLL).

Table 1: Sources of systematic uncertainty and their treatment in S2 for the extrapolation of the SM cross-section measurement and the resonance search in the 2LSS/ML channel. "Mat. Conv." and "Low $m_{\gamma*}$" refer respectively to events with one non-prompt electron originating from photon conversion in the detector material and to events with a virtual photon leading to an e^+e^- pair.

Uncertainty source	**Treatment in S2**
Signal modelling	
$t\bar{t}t\bar{t}$ Parton shower	Half of Run 2
$t\bar{t}t\bar{t}$ Generator	Removed
$t\bar{t}t\bar{t}$ EW	Half of Run 2
$t\bar{t}t\bar{t}$ Renormalisation and factorisation scales	Half of Run 2
Cross-section	Half of Run 2
Background modelling	
$t\bar{t}W$**+jets modelling**	
Renormalisation and factorisation scales	Half of Run 2
Generator	Half of Run 2
Additional heavy-flavour jets	Scaled by luminosity
Cross-section	Half of Run 2
7/≥ 8 jets normalisation (resonance search only)	Same as Run 2
$t\bar{t}t$ **modelling**	
Additional heavy-flavour jets	Scaled by luminosity
Cross-section	Half of Run 2
Non-prompt leptons modelling	Scaled by luminosity
$t\bar{t}H$**+jets and** $t\bar{t}Z$**+jets modelling**	
Generator	Half of Run 2
PDF	Half of Run 2
Renormalisation and factorisation scales	Half of Run 2
Additional heavy-flavour jets	Scaled by luminosity
Cross-section	Half of Run 2
Other background modelling	
Additional heavy-flavour jets	Half of Run 2
Cross-section	Scaled by luminosity
Charge misassignment	Same as Run 2
Template fit shape uncertainties	
Mat. Conv., $\gamma*$, and non-prompt leptons	Scaled by luminosity
Other fake leptons	Half of Run 2
Additional heavy-flavour jets	Half of Run 2
Instrumental	Scaled by luminosity

3.2 Extrapolation of the top-quark Yukawa coupling measurement and of limits on effective field theory operators

The top-quark Yukawa coupling plays a crucial role in electroweak interactions involving top quarks. In particular, it enters the Feynman diagrams for processes where a pair of top quarks is produced via the decay of an off-shell Higgs boson. This makes $t\bar{t}t\bar{t}$ production inherently sensitive to the top-quark Yukawa coupling, influencing both its strength and its CP properties. Additionally, the top-quark Yukawa coupling also affects the $t\bar{t}H$+jets process, which is a background for $t\bar{t}t\bar{t}$ production. The cross-section for $t\bar{t}t\bar{t}$ production can be expressed as a function of the top-quark Yukawa coupling strength modifier, κ_t, assuming a CP-even coupling as in the SM. The modifier κ_t is defined as the ratio of the actual top-quark Yukawa coupling, y_t to its SM prediction, y_t^{SM}. Hence, κ_t is 1 in the SM. The $t\bar{t}H$+jets cross-section

Table 2: Sources of systematic uncertainty considered in the 1L/2LOS-channel analysis and their treatment in S2.

Uncertainty source	**Treatment in S2**
BSM $t\bar{t}t\bar{t}$ modelling	
PDF	Half of Run 2
Renormalisation and factorisation scales	Half of Run 2
SM $t\bar{t}t\bar{t}$ background modelling	
Parton shower	Half of Run 2
Generator	Half of Run 2
Renormalisation and factorisation scales	Half of Run 2
Cross-section	Half of Run 2
Other background modelling	
$t\bar{t}$ modelling	
Parton shower	Half of Run 2
Generator	Half of Run 2
4FS vs 5FS	Half of Run 2
NN kinematic corrections	Scaled by luminosity
Cross-section	Half of Run 2
$t\bar{t}W$ and $t\bar{t}H$ modelling	
Generator	Half of Run 2
Renormalisation and factorisation scales	Half of Run 2
Cross-section	Half of Run 2
N_{jets} mismodelling	Same as Run 2
$t\bar{t}Z$ modelling	
Renormalisation and factorisation scales	Half of Run 2
Cross-section	Half of Run 2
N_{jets} mismodelling	Same as Run 2
Single Top modelling	
ME and PS choice	Half of Run 2
DR/DS scheme	Half of Run 2
Renormalisation and factorisation scales	Half of Run 2
Cross-section	Half of Run 2
V+jet, $t\bar{t}$, others modelling	
Cross-section	Half of Run 2
Instrumental	Scaled by luminosity

also depends on this parameter. However, unlike $t\bar{t}t\bar{t}$ production, the kinematic distributions in $t\bar{t}H$+jets events remain unchanged unless a CP-odd term is non-zero. Figure 2 presents the expected experimental uncertainty on y_t as a function of the integrated luminosity, comparing the two scenarios for uncertainty scaling used in the cross-section extrapolation. The extrapolation is carried out either by parameterizing $t\bar{t}H$+jets events as a function of κ_t or by allowing the $t\bar{t}H$+jets contribution to float freely, ie. without any assumption on the Higgs width that would be present when using $t\bar{t}H$+jets events. In S2, an uncertainty of approximately 0.11 could be achieved with 3 ab^{-1} per experiment.

Within the framework of EFT, the $t\bar{t}t\bar{t}$ production process is particularly sensitive to four heavy-flavour fermion operators: O^1_{tt}, O^1_{QQ}, O^1_{Qt}, and O^8_{Qt} [40]. These operators include both color-singlet (^{1}) and color-octet (^{8}) structures, where Q represents a generic quark. These operators provide a powerful probe of BSM scenarios that enhance interactions between third-generation quarks. The impact of these operators

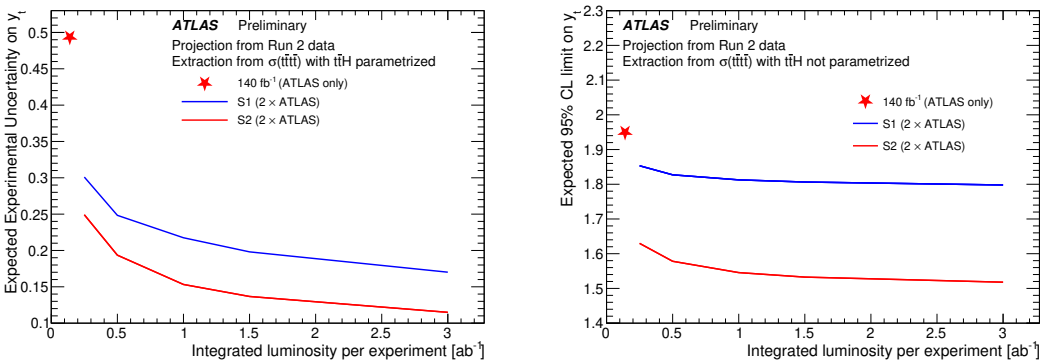

Figure 2: Expected experimental uncertainty on y_t as a function of the integrated luminosity per experiment. The blue and red curves correspond to two different scenarios of systematic uncertainty treatment (S1 and S2). The red star represents the ATLAS-only result using 140 fb^{-1} [2] from Run 2. The precision of the combined ATLAS and CMS result is approximated by doubling the integrated luminosity of a single experiment. The plot on the left is obtained when the $t\bar{t}H$+jets events are parametrized as a function of κ_t, while the plot on the right is obtained when the $t\bar{t}H$+jets contribution is freely floating.

manifests by modifying the $t\bar{t}t\bar{t}$ production cross-section, which can be approximated by:

$$\sigma_{t\bar{t}t\bar{t}} = \sigma^{SM}_{t\bar{t}t\bar{t}} + \frac{1}{\Lambda^2}\sum_i C_i\sigma_i^{(1)} + \frac{1}{\Lambda^4}\sum_{i\leq j} C_iC_j\sigma_{i,j}^{(2)}, \tag{1}$$

where C_i denotes the Wilson coefficient of the four heavy-flavour fermion operators, and Λ corresponds to the cut-off scale of the effective theory. The term $C_i\sigma_i^{(1)}$ represents the contribution of the leading order of the dimension-6 operators, while $C_iC_i\sigma_{i,j}^{(2)}$ includes additional contributions from the dimension-8 effects and interactions between different EFT operators. These terms modify the SM cross-section, incorporating potential effects from BSM interactions.

The expected 95% CL intervals on the EFT Wilson coefficients, assuming a single parameter variation in the fit, are summarized in Table 3, extrapolating the results obtained using the SM GNN from the Run 2 analysis. The results are shown for the two uncertainty scenarios described above and extrapolated to integrated luminosities of 2 ab^{-1} and 3 ab^{-1} per experiment. Furthermore, expected limits are compared to published constraints using 140 fb^{-1} of ATLAS data [2], providing a direct evaluation of improvements with increased luminosity.

The limits show a substantial improvement over the current ATLAS-only results. For example, the constraints on O^8_{Qt} tighten from [-4.3, 5.1] to [-1.9, 2.7], while those on O^1_{tt} shrink from [-1.2, 1.4] to [-0.5, 0.8] at 3 ab^{-1} per experiment in Scenario 2. However, the gain from 2 ab^{-1} per experiment is minimal in both scenarios, indicating that most of the sensitivity improvement is already achieved at this luminosity. Scenario 2 consistently provides stronger constraints than Scenario 1, emphasizing the impact of uncertainty treatment. The expected C_i/Λ^2 as a function of the integrated luminosity per experiment for O^8_{Qt} is presented in Figure 3, illustrating the potential of HL-LHC to significantly refine these constraints.

These projections are based on the Run 2 analysis strategy, utilizing the GNN discriminant developed for the SM measurement of the inclusive $t\bar{t}t\bar{t}$ cross-section [2] and not optimized for EFT sensitivity to extract the EFT limits. Since this discriminant is optimized for distinguishing $t\bar{t}t\bar{t}$ from background processes rather than specifically enhancing sensitivity to high-H_T regions, the obtained limits are expected to be

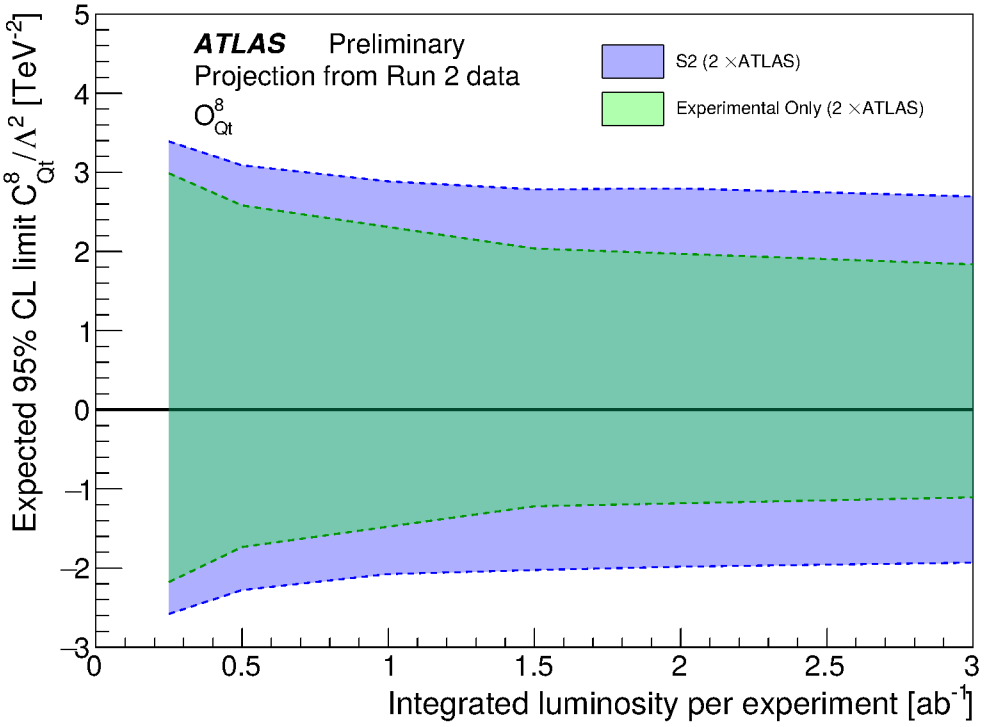

Figure 3: Expected C_i/Λ^2 exclusion as a function of integrated luminosity per experiment, for the SMEFT operator O^8_{Qt}. Results are shown for S2. The precision of the combined ATLAS and CMS result is approximated by doubling the integrated luminosity of a single experiment. The impact of the experimental and total uncertainties are shown separately.

conservative. A dedicated approach incorporating discriminants explicitly tuned to EFT effects could potentially yield stronger constraints. To illustrate this, Figure 4 shows the expected reconstruction-level distribution of the H_T variable for 3 ab^{-1} per experiment. The selection requires two same-sign leptons or three leptons, along with at least six jets, including four b-tagged jets in the signal region. In the Run 2 analysis, the background is found to be negligible after this requirement. This extrapolation shows that around 33 events are expected to have $H_T > 1.5$ TeV. It also shows that using this distribution to constrain the EFT parameters could lead to a stronger bound. In fact, in particular, for the operator O^8_{Qt}, a clear difference is found from the SM expectation for a coefficient set to the S2 limit from Table 3 for O^8_{Qt}.

3.3 Search for heavy resonance particles in $t\bar{t}t\bar{t}$ topologies

The projection is performed under the background-only hypothesis, setting exclusion limits at the 95% confidence level (CL) on the production cross-sections and relevant model parameters of the heavy resonance signals under consideration. Upper limits on the cross-sections are projected for the heavy H/A in 2HDM and the colour-octet scalar (S_8) predicted in Ref. [10] that are considered in the ATLAS Run 2 search [36]. The upper bound of the probed $m_{H/A}$ is extended from 1 TeV to 1.5 TeV. In addition, the colour-singlet scalar (S_1) from Ref. [10] is also considered for the projection. Limits are set for both the production cross-sections and the mass and the coupling of S_1 with the top quark, y_{S_1}. For all projected

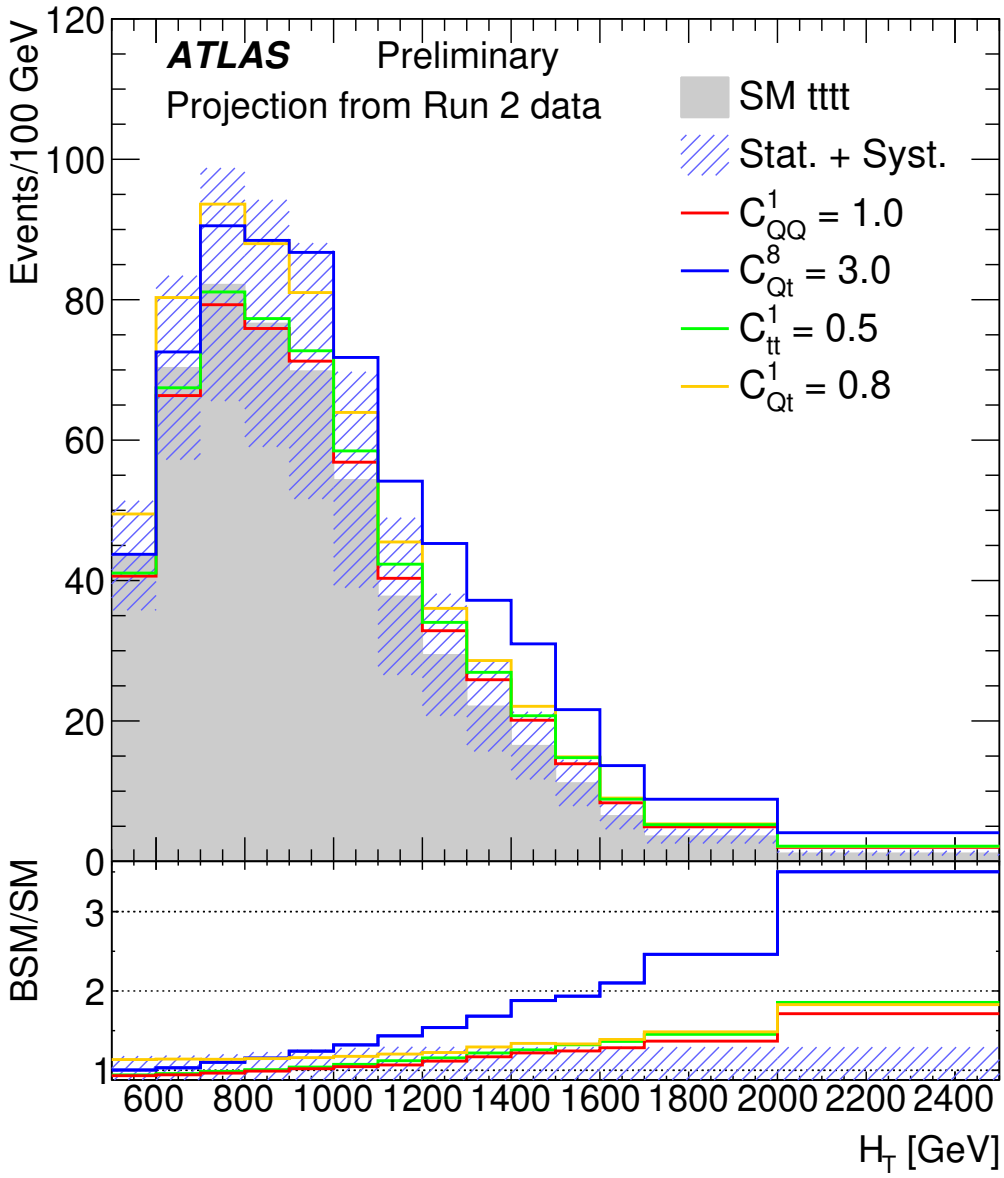

Figure 4: Expected reconstruction-level distribution of the H_T variable for events passing the selection criteria: two same-sign leptons or three leptons, at least six jets, and four b-tagged jets. The H_T distributions for the EFT four-heavy fermion Wilson coefficients are set to values close to the expected limits with 3 ab^{-1} per experiment, using Λ = 1 TeV. The precision of the combined ATLAS and CMS result is approximated by doubling the integrated luminosity of a single experiment. The hashed band indicates the total uncertainty, including both statistical and systematic components.

results, the MVA used is the one from the original analyses optimised for the $t\bar{t}H/A \rightarrow t\bar{t}t\bar{t}$ signals up to $m_{H/A}$ = 1 TeV. No dedicated re-optimisation for the additional BSM signals were performed. For all signals with a resonance mass greater than 1 TeV, the MVA optimised for $m_{H/A}$ = 1 TeV is used.

Figure 5 shows the expected upper limit on the $t\bar{t}H/A$ production cross-section, $\sigma(pp \rightarrow t\bar{t}H/A)$, times

Table 3: Expected 95% CL intervals on EFT Wilson coefficients, assuming a single non-zero EFT parameter at a time. The ATLAS-only result uses 140 fb^{-1} [2] from Run 2. Results are shown for the two uncertainty treatment scenarios and extrapolated to integrated luminosities per experiment of 2 ab^{-1} and 3 ab^{-1}. The precision of the combined ATLAS and CMS result is approximated by doubling the integrated luminosity of a single experiment.

Operators	Expected $C_i/\Lambda^2[TeV^{-2}]$ 140 fb^{-1} ATLAS Only	Scenario 1 2 ab^{-1}	Scenario 1 3 ab^{-1}	Scenario 2 2 ab^{-1}	Scenario 2 3 ab^{-1}
O^1_{QQ}	[-2.5, 3.2]	[-1.9, 2.5]	[-1.9, 2.5]	[-1.1, 1.7]	[-1.1, 1.7]
O^1_{Qt}	[-2.6, 2.1]	[-2.0, 1.6]	[-2.0, 1.6]	[-1.4, 0.9]	[-1.4, 0.9]
O^1_{tt}	[-1.2, 1.4]	[-0.9, 1.1]	[-0.9, 1.1]	[-0.5, 0.8]	[-0.5, 0.8]
O^8_{Qt}	[-4.3, 5.1]	[-3.4, 4.1]	[-3.4, 4.1]	[-2.0, 2.8]	[-1.9, 2.7]

the $H/A \to t\bar{t}$ branching fraction, $B(H/A \to t\bar{t})$, at 95% CL. The result using ATLAS Run 2 data is compared with projections for the ATLAS and CMS combination at integrated luminosities of 2 ab^{-1} and 3 ab^{-1} per experiment under the two scenarios. The reduced systematic uncertainties from S2 show a larger effect than the increase of the integrated luminosity from 2 ab^{-1} to 3 ab^{-1}. At lower mass points, the former leads to a 30% improvement, while the latter's effect is roughly 10%. The increased integrated luminosity becomes more important at higher mass points due to the reduced impact of the systematic uncertainties. Figure 6 and 7 show similar projections for the S_8 and S_1 scalars. As opposed to the colour-singlet scalars H/A and S_1, the main production mode for the S_8 scalar with a mass $m_{S_8} < 2$ TeV is $gg \to S_8S_8$, where S_8 decays to a $t\bar{t}$ pair. The cross-section and kinematics of the S_1 production events are affected not only by its mass but also by the coupling between S_1 and the top quark, y_{S_1}, mainly through the mass width of the S_1 scalar. The width of S_1 ranges from below 1 GeV for $y_{S_1} = 0.1$ to 25 GeV for $y_{S_1} = 2.0$ at the 400 GeV mass point. The width increases for higher mass points. At 2 TeV, the width ranges from 10 GeV to 900 GeV. Upper limits on $\sigma(pp \to t\bar{t}S_1) \times B(S_1 \to t\bar{t})$ are shown for $y_{S_1} = 0.1$ and $y_{S_1} = 2.0$. In general, the limits present similar behaviour as those for H/A and S_8. The limits become slightly worse for larger widths. The cross-section upper limits are compared to the predicted cross-sections to obtain exclusion in the two-dimensional plane of (m_{S_1}, y_{S_1}), as shown in Figure 8. With the combination of ATLAS and CMS datasets and 3 ab^{-1} from each experiment under S2, the most stringent limit is obtained at $m_{S_1} = 400$ GeV, where all values of $y_{S_1} > 0.17$ are excluded. For higher mass points, the exclusion becomes weaker due to the much smaller predicted cross-sections, despite the more stringent limits in the cross-sections. For $m_{S_1} = 1.5$ TeV, values of $y_{S_1} > 0.8$ (0.95) are excluded with 3 ab^{-1} under S2 (2 ab^{-1} under S1).

To demonstrate the evolution of the search sensitivity with increasing integrated luminosity, Figure 9 illustrates, as an example, the upper limit on the $pp \to t\bar{t}H/A \to t\bar{t}t\bar{t}$ cross-section as a function of the integrated luminosity. The lowest and highest mass points, 400 GeV and 1.5 TeV, are shown, and the two scenarios S1 and S2 are compared. For the 400 GeV $t\bar{t}H/A$ signal and above 1 ab^{-1}, the effects from the systematic uncertainties become dominant over the increase in the integrated luminosity. However, for the high mass points, the gain in sensitivity due to the increased luminosity and the combination of the ATLAS and CMS dataset is still sizable.

The search sensitivities to injected $t\bar{t}H/A \to t\bar{t}t\bar{t}$ signals with $m_{H/A} = 400$, 800 and 1500 GeV are evaluated. The injected signals correspond to $\sigma(pp \to t\bar{t}H/A) \times B(H/A \to t\bar{t})$ of 6.1, 3.3 and 2.0 fb, respectively. The values are chosen such that, with 1 ab^{-1} of data from each experiment under S2, the local significance reaches three standard deviations (σ). The presence of these signals is consistent with the current ATLAS and CMS resonance search results where none of these signals exceed a local significance

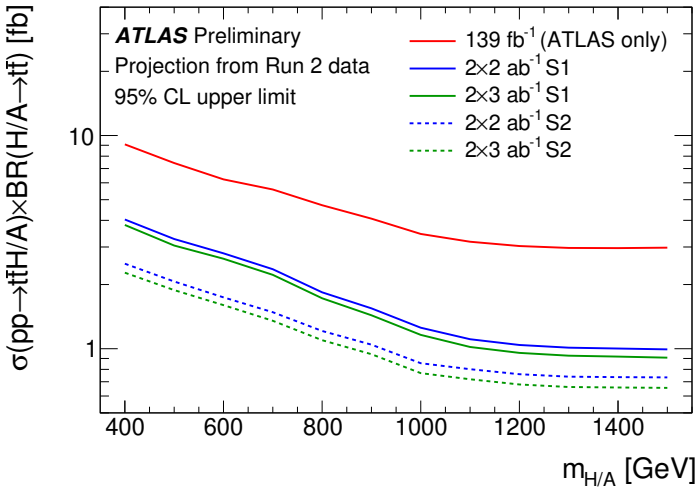

Figure 5: Expected 95% CL upper limits on the cross-section times branching ratio, $\sigma(pp \to t\bar{t}H/A) \times B(H/A \to t\bar{t})$, as a function of $m_{H/A}$ obtained from different datasets and scenarios. The solid red line shows the expected upper limits using ATLAS Run 2 data. The blue and green lines show the projections for the integrated luminosity of 2 ab^{-1} and 3 ab^{-1} per experiment, respectively. The precision of the combined ATLAS and CMS result is approximated by doubling the integrated luminosity of a single experiment. The solid (dashed) line corresponds to S1 (S2).

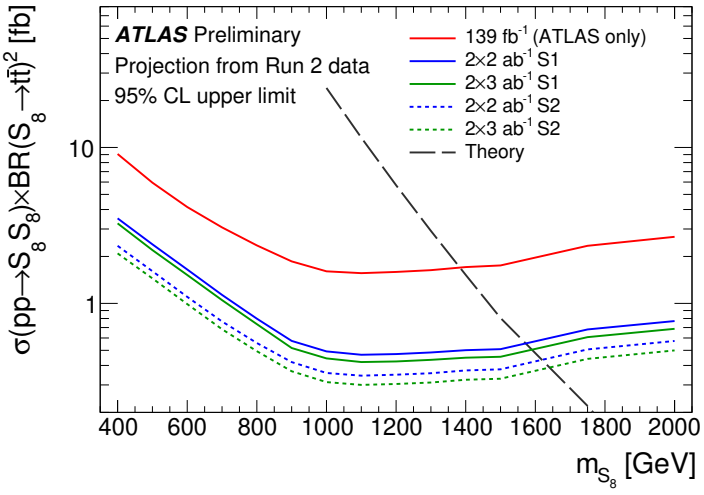

Figure 6: Expected 95% CL upper limits on the cross-section times branching ratio, $\sigma(pp \to S_8 S_8) \times B(S_8 \to t\bar{t})^2$, as a function of m_{S_8} obtained from different datasets and scenarios. The solid red line shows the expected upper limits using ATLAS Run 2 data. The blue and green lines show the projections for the integrated luminosity of 2 ab^{-1} and 3 ab^{-1} per experiment, respectively. The precision of the combined ATLAS and CMS result is approximated by doubling the integrated luminosity of a single experiment. The solid (dashed) line corresponds to S1 (S2).

of 2 σ [36]. The local significances of the injected signals reach 4.7, 5.0 and 4.9 σ with 2 ab^{-1} of data from each experiment under S2, whilst with 3 ab^{-1}, the expected local significances are 5.2, 5.4 and 5.5 σ.

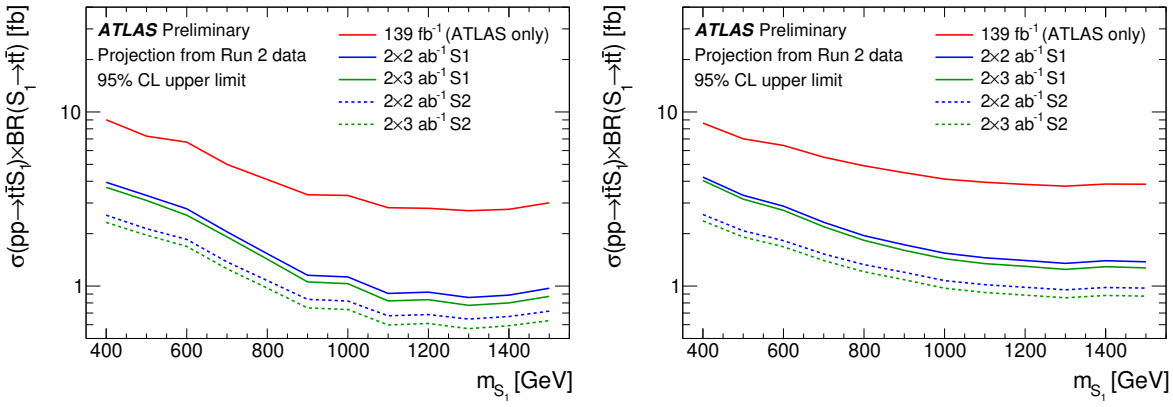

(a) (b)

Figure 7: Expected 95% CL upper limits on the cross-section times branching ratio, $\sigma(pp \to t\bar{t}S_1) \times B(S_1 \to t\bar{t})$, as a function of m_{S_1}, for (a) $y_{S_1} = 0.1$ and (b) $y_{S_1} = 2.0$, obtained from different datasets and scenarios. The solid red line shows the expected upper limits using ATLAS Run 2 data. The blue and green lines show the projections for the integrated luminosity of 2 ab^{-1} and 3 ab^{-1} per experiment, respectively. The precision of the combined ATLAS and CMS result is approximated by doubling the integrated luminosity of a single experiment. The solid (dashed) line corresponds to S1 (S2). The mild irregularities in the limits arise from the limited size of the MC samples.

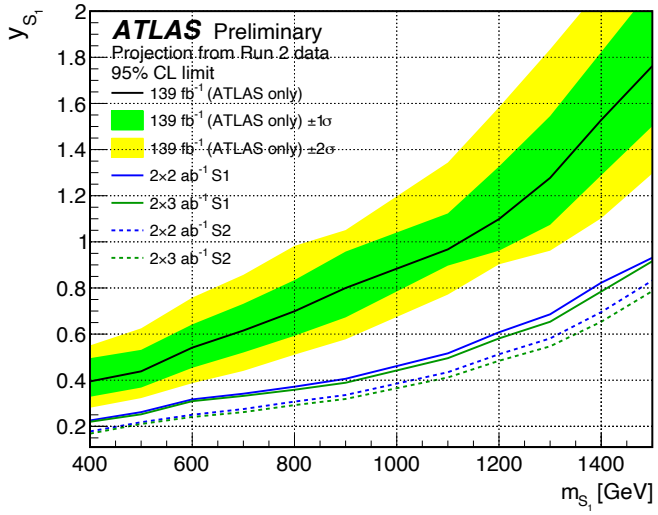

Figure 8: Expected 95% CL limits on m_{S_1} and y_{S_1}, obtained assuming $B(S_1 \to t\bar{t}) = 1$ for different datasets and scenarios. The area above the lines is excluded. The solid black line shows the expected upper limits using ATLAS Run 2 data, with the yellow and green band illustrating the one and two standard deviations. The blue and green lines show the projections for the integrated luminosity of 2 ab^{-1} and 3 ab^{-1} per experiment, respectively. The precision of the combined ATLAS and CMS result is approximated by doubling the integrated luminosity of a single experiment. The solid (dashed) line corresponds to S1 (S2).

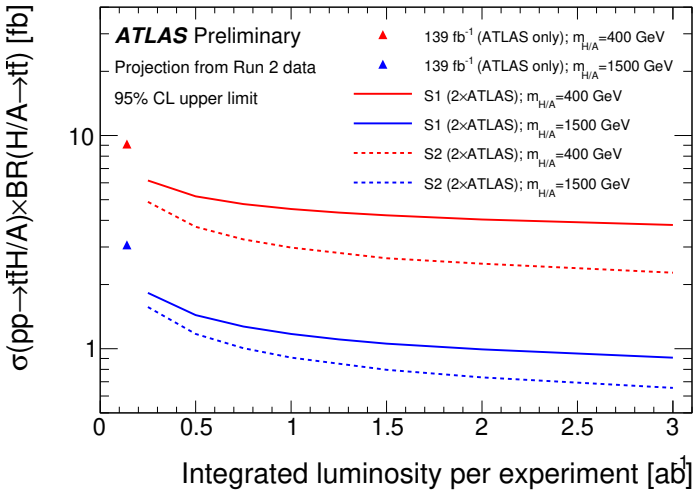

Figure 9: Expected 95% CL upper limits on the cross-section times branching ratio, $\sigma(pp \to t\bar{t}H/A) \times B(H/A \to t\bar{t})$, as a function of the integrated luminosity per experiment. The precision of the combined ATLAS and CMS result is approximated by doubling the integrated luminosity of a single experiment. The red (blue) lines and markers illustrate the results for $m_{H/A}$ = 400 GeV ($m_{H/A}$ = 1500 GeV). The markers represent the results obtained using ATLAS Run 2 data. The solid (dashed) lines correspond to the projections under S1 (S2).

4 Conclusion

The expected sensitivities for measuring the SM $t\bar{t}t\bar{t}$ production cross-section and probing new physics scenarios at the HL-LHC have been estimated. Extrapolations are based on results obtained using ATLAS Run 2 data [2, 36], extended to the 3 ab^{-1} dataset anticipated at $\sqrt{s}$ = 14 TeV both for the ATLAS and CMS experiments.

Two scenarios are considered, differing in their assumptions about the evolution of systematic uncertainties. The conservative scenario, S1, retains the systematic uncertainties observed in the 140 fb^{-1} analysis at $\sqrt{s}$ = 13 TeV. The more optimistic scenario, S2, assumes improvements in systematic uncertainties.

The projection suggests that with 3 ab^{-1}, the uncertainty in measuring the $t\bar{t}t\bar{t}$ cross-section could decrease to 17%, with potential further reductions to 7% through better control of systematic uncertainties. A combined ATLAS and CMS analysis could reduce the uncertainty to 6%. In the best scenario, an uncertainty of approximately 0.11 on y_t could be achieved by combining the ATLAS and CMS results when parameterising the $t\bar{t}H$+jets contribution. The expected limits on EFT operators also show a significant improvement over current ATLAS-only results in S2. However, even with the full HL-LHC dataset, differential measurements of this process will remain statistically limited, highlighting the importance of maximizing data-driven and theoretical improvements to fully exploit the potential of future analyses.

The extrapolated sensitivities for the resonance searches reach below 1 fb for most resonance particles with a mass beyond 1 TeV in S1. The most stringent cross-section upper limit is expected for the pair production of the colour-octet scalar, S_8, with a mass around 1.2 TeV, reaching 0.3 fb. The difference in expected sensitivities between S1 and S2 highlights the importance of improved systematic uncertainties for resonances below 1 TeV. For higher resonance masses, the total integrated luminosity from the HL-LHC becomes increasingly critical in enhancing search sensitivity.

References

[1] M. van Beekveld, A. Kulesza and L. M. Valero,
Threshold resummation for the production of four top quarks at the LHC,
Phys. Rev. Lett. **131** (2022), arXiv: 2212.03259 [hep-ph] (cit. on p. 2).

[2] ATLAS Collaboration,
Observation of four-top-quark production in the multilepton final state with the ATLAS detector,
Eur. Phys. J. C **83** (2023) 496, arXiv: 2303.15061 [hep-ex] (cit. on pp. 2–4, 7, 10, 13),
Erratum: Eur. Phys. J. C **84** (2024) 156.

[3] A. Hayrapetyan et al.,
Observation of four top quark production in proton-proton collisions at s=13TeV,
Phys. Lett. B **847** (2023) 138290, arXiv: 2305.13439 [hep-ex] (cit. on p. 2).

[4] R. Aoude, H. El Faham, F. Maltoni and E. Vryonidou,
Complete SMEFT predictions for four top quark production at hadron colliders,
JHEP **10** (2022) 163, arXiv: 2208.04962 [hep-ph] (cit. on p. 2).

[5] G. C. Branco et al., *Theory and phenomenology of two-Higgs-doublet models*,
Phys. Rept. **516** (2012) 1, arXiv: 1106.0034 [hep-ph] (cit. on p. 2).

[6] N. Greiner, K. Kong, J.-C. Park, S. C. Park and J.-C. Winter,
Model-independent production of a top-philic resonance at the LHC, JHEP **04** (2015) 029,
arXiv: 1410.6099 [hep-ph] (cit. on p. 2).

[7] J. H. Kim, K. Kong, S. J. Lee and G. Mohlabeng,
Probing TeV scale top-philic resonances with boosted top-tagging at the high luminosity LHC,
Phys. Rev. D **94** (3 2016) 035023, arXiv: 1604.07421 [hep-ph] (cit. on p. 2).

[8] P. J. Fox, I. Low and Y. Zhang, *Top-philic Z' forces at the LHC*, JHEP **03** (2018) 074,
arXiv: 1801.03505 [hep-ph] (cit. on p. 2).

[9] E. Alvarez, D. A. Faroughy, J. F. Kamenik, R. Morales and A. Szynkman, *Four tops for LHC*,
Nucl. Phys. B **915** (2017) 19, arXiv: 1611.05032 [hep-ph] (cit. on p. 2).

[10] L. Darmé, B. Fuks and F. Maltoni,
Top-philic heavy resonances in four-top final states and their EFT interpretation,
JHEP **09** (2021) 143, arXiv: 2104.09512 [hep-ph] (cit. on pp. 2, 8).

[11] B. Lillie, J. Shu and T. M. Tait, *Top Compositeness at the Tevatron and LHC*, JHEP **04** (2008) 087,
arXiv: 0712.3057 [hep-ph] (cit. on p. 2).

[12] A. Pomarol and J. Serra, *Top Quark Compositeness: Feasibility and Implications*,
Phys. Rev. D **78** (2008) 074026, arXiv: 0806.3247 [hep-ph] (cit. on p. 2).

[13] N. Zhou, D. Whiteson and T. M. Tait,
Limits on Four-Top Production from the ATLAS Same-sign Top-quark Search,
Phys. Rev. D **85** (2012) 091501, arXiv: 1203.5862 [hep-ph] (cit. on p. 2).

[14] G. Cacciapaglia et al., *Composite scalars at the LHC: the Higgs, the Sextet and the Octet*,
JHEP **11** (2015) 201, arXiv: 1507.02283 [hep-ph] (cit. on p. 2).

[15] D. Liu, L.-T. Wang and K.-P. Xie, *Broad composite resonances and their signals at the LHC*,
Phys. Rev. D **100** (2019) 075021, arXiv: 1901.01674 [hep-ph] (cit. on p. 2).

[16] G. Cacciapaglia, A. Deandrea, T. Flacke and A. Iyer,
Gluon-Photon Signatures for color octet at the LHC (and beyond), JHEP **05** (2020) 027,
arXiv: 2002.01474 [hep-ph] (cit. on p. 2).

[17] M. Gerbush, T. J. Khoo, D. J. Phalen, A. Pierce and D. Tucker-Smith,
Color-octet scalars at the CERN LHC, Phys. Rev. D **77** (2008) 095003,
arXiv: 0710.3133 [hep-ph] (cit. on p. 2).

[18] A. Hayreter and G. Valencia, *LHC constraints on color octet scalars*,
Phys. Rev. D **96** (2017) 035004, arXiv: 1703.04164 [hep-ph] (cit. on p. 2).

[19] A. Salam and J. A. Strathdee, *Supersymmetry and Fermion Number Conservation*,
Nucl. Phys. B **87** (1975) 85 (cit. on p. 2).

[20] P. Fayet, *Supergauge Invariant Extension of the Higgs Mechanism and a Model for the electron and Its Neutrino*, Nucl. Phys. B **90** (1975) 104 (cit. on p. 2).

[21] P. Fayet, *Fermi-Bose Hypersymmetry*, Nucl. Phys. B **113** (1976) 135 (cit. on p. 2).

[22] L. Alvarez-Gaume and S. F. Hassan, *Introduction to S duality in N=2 supersymmetric gauge theories: A Pedagogical review of the work of Seiberg and Witten*, Fortsch. Phys. **45** (1997) 159,
arXiv: hep-th/9701069 (cit. on p. 2).

[23] P. J. Fox, A. E. Nelson and N. Weiner,
Dirac gaugino masses and supersoft supersymmetry breaking, JHEP **08** (2002) 035,
arXiv: hep-ph/0206096 (cit. on p. 2).

[24] T. Plehn and T. M. Tait, *Seeking Sgluons*, J. Phys. G **36** (2009) 075001,
arXiv: 0810.3919 [hep-ph] (cit. on p. 2).

[25] S. Choi et al., *Color-Octet Scalars of N=2 Supersymmetry at the LHC*, Phys. Lett. B **672** (2009) 246,
arXiv: 0812.3586 [hep-ph] (cit. on p. 2).

[26] D. Goncalves-Netto, D. Lopez-Val, K. Mawatari, T. Plehn and I. Wigmore,
Sgluon Pair Production to Next-to-Leading Order, Phys. Rev. D **85** (2012) 114024,
arXiv: 1203.6358 [hep-ph] (cit. on p. 2).

[27] B. Fuks, *Beyond the Minimal Supersymmetric Standard Model: from theory to phenomenology*,
Int. J. Mod. Phys. A **27** (2012) 1230007, arXiv: 1202.4769 [hep-ph] (cit. on p. 2).

[28] S. Calvet, B. Fuks, P. Gris and L. Valery,
Searching for sgluons in multitop events at a center-of-mass energy of 8 TeV, JHEP **04** (2013) 043,
arXiv: 1212.3360 [hep-ph] (cit. on p. 2).

[29] K. Benakli, M. Goodsell, F. Staub and W. Porod,
Constrained minimal Dirac gaugino supersymmetric standard model,
Phys. Rev. D **90** (2014) 045017, arXiv: 1403.5122 [hep-ph] (cit. on p. 2).

[30] L. Beck et al., *Probing top-philic sgluons with LHC Run I data*, Phys. Lett. B **746** (2015) 48,
arXiv: 1501.07580 [hep-ph] (cit. on p. 2).

[31] W. Kotlarski, *Sgluons in the same-sign lepton searches*, JHEP **02** (2017) 027,
arXiv: 1608.00915 [hep-ph] (cit. on p. 2).

[32] L. Darmé, B. Fuks and M. Goodsell, *Cornering sgluons with four-top-quark events*,
Phys. Lett. B **784** (2018) 223, arXiv: 1805.10835 [hep-ph] (cit. on p. 2).

[33] L. M. Carpenter, T. Murphy and M. J. Smylie,
Exploring color-octet scalar parameter space in minimal R-symmetric models, JHEP **11** (2020) 024, arXiv: 2006.15217 [hep-ph] (cit. on p. 2).

[34] L. M. Carpenter and T. Murphy,
Color-octet scalars in Dirac gaugino models with broken R symmetry, JHEP **05** (2021) 079, arXiv: 2012.15771 [hep-ph] (cit. on p. 2).

[35] I. Zurbano Fernandez et al.,
High-Luminosity Large Hadron Collider (HL-LHC): Technical design report, **10/2020** (2020), ed. by I. Béjar Alonso et al. (cit. on p. 2).

[36] ATLAS Collaboration, *Search for $t\bar{t}H/A \to t\bar{t}t\bar{t}$ production in proton–proton collisions at $\sqrt{s} = 13$ TeV with the ATLAS detector*, (2024), arXiv: 2408.17164 [hep-ex] (cit. on pp. 2, 3, 8, 11, 13).

[37] ATLAS Collaboration, *Search for $t\bar{t}H/A \to t\bar{t}t\bar{t}$ production in the multilepton final state in proton–proton collisions at $\sqrt{s} = 13$ TeV with the ATLAS detector*, JHEP **07** (2023) 203, arXiv: 2211.01136 [hep-ex] (cit. on pp. 2, 3).

[38] P. W. Battaglia et al., *Relational inductive biases, deep learning, and graph networks*, (2018), arXiv: 1806.01261 [cs.LG] (cit. on p. 3).

[39] R. Frederix, D. Pagani and M. Zaro, *Large NLO corrections in $t\bar{t}W^{\pm}$ and $t\bar{t}t\bar{t}$ hadroproduction from supposedly subleading EW contributions*, JHEP **02** (2018) 031, arXiv: 1711.02116 [hep-ph] (cit. on p. 4).

[40] C. Zhang,
Constraining qqtt operators from four-top production: a case for enhanced EFT sensitivity, Chin. Phys. C **42** (2018) 023104, arXiv: 1708.05928 [hep-ph] (cit. on p. 6).